

# Unsupervised Segmentation of Retinal Blood Vessels using a Single Parameter Vesselness Measure

Nancy M. Salem and Asoke K. Nandi

Signal Processing and Communications Group,

Department of Electrical Engineering and Electronics,

The University of Liverpool. Brownlow Hill, L69 3GJ, Liverpool, UK

**Abstract—**In this paper, a novel vesselness measure based on analysis of the Hessian matrix is presented. The larger eigenvalue of the Hessian matrix is used for vessel centerlines detection, while vessel orientations are estimated from the eigenvectors corresponding to the smaller eigenvalue. The vesselness measure combines information from vessel centerlines and orientations over scales to segment retinal blood vessels from colour fundus images. A publicly available dataset is used to evaluate the performance of our proposed method which has the advantage of being unsupervised and of using only one parameter.

## I. INTRODUCTION

Automated analysis of retinal images is a challenging research area that aims to provide automated methods to help in the early detection and diagnosis of many eye diseases such as diabetic retinopathy and age-related macular degeneration (AMD). Retinal image pre-processing, segmentation, and analysis benefit from different forms of contributions from digital image processing techniques in this area.

Automated segmentation of retinal blood vessels is an important step in screening programs for diabetic retinopathy [1], evaluation of the retinopathy of prematurity [2], registration of retinal images for treatment evaluation (to follow the evaluation of some lesions over time or to compare images obtained under different conditions) [3], [4], generating retinal map for the diagnosis and treatment of AMD [5], or locating the optic disc [6], [7] and the fovea [8].

Methods for blood vessels segmentation of retinal images, according to the classification method, can be divided into two groups - supervised and unsupervised methods. Supervised methods, which require feature vectors for each pixel and manually labelled images for training, use the neural networks [1], the  $K$ -nearest neighbour classifier [9], [10], [11], or the Bayesian classifier [12] for classifying image pixels as blood vessel or non-blood vessel pixels. These methods depend on generating a feature vector for every pixel in the image and then using training samples (with known classes) to design a classifier to classify these training samples into their corresponding classes.

Unsupervised methods in the literature comprise the matched filter response [13], [14], [15], grouping of edge pixels [5], adaptive thresholding [16], [17], vessel tracking [17], [18], topology adaptive snakes [19], and morphology based techniques [20], [21].

The two dimensional matched filter proposed in [13] assumes the blood vessels are of constant width but may be of different orientations, so it uses fixed values for parameters which was subsequently improved in [15], where the parameters for the matched filter are varied and chosen according to an optimisation procedure. In the piecewise threshold probing proposed in [14], the matched filter response image, resulting from convolution with matched filter in [13], is probed. During each probing, the threshold of the probed region is determined according to testing a set of criteria, and ultimately it is decided if the area being probed was a blood vessel or not. The work in [16] is based on a verification based multithreshold probing scheme. In which a binary image is obtained at each of the different threshold values and each time vessels are selected based on verification steps.

The Hessian matrix is used for ridge detection to extract vessel centerlines [9], [22]. The eigenvalue analysis of the Hessian matrix have been used to develop a line-enhancement filter which applied on 2D and 3D medical images such as digital subtraction angiography (DSA) and magnetic resonance angiography (MRA) from brain blood vessels, aortoiliac MRA and computed tomography (CT) from lungs [23], [24], [25].

In this paper, we introduce an unsupervised method for segmentation of retinal blood vessels from colour fundus images. Blood vessels centerlines and orientations are used to quantify the vesselness measure. The main advantage of our proposed method is that it is completely unsupervised, so there is no need for manually labelled images which is time consuming and require an expert. This paper is organised as follows. In section 2, the proposed method is detailed, while section 3 presents the dataset. Experimental results are presented in section 4. Results are discussed in section 5 and conclusions are drawn in section 6.

## II. PROPOSED SEGMENTATION METHOD

### A. Preprocessing of Retinal Images

Unsupervised methods for segmenting blood vessels in colour fundus images use the green channel [9], [10], [13], [14], [15], [16], because generally it has the highest contrast between blood vessels and the retinal background while the red channel is rather saturated and the blue channel is rather dark.

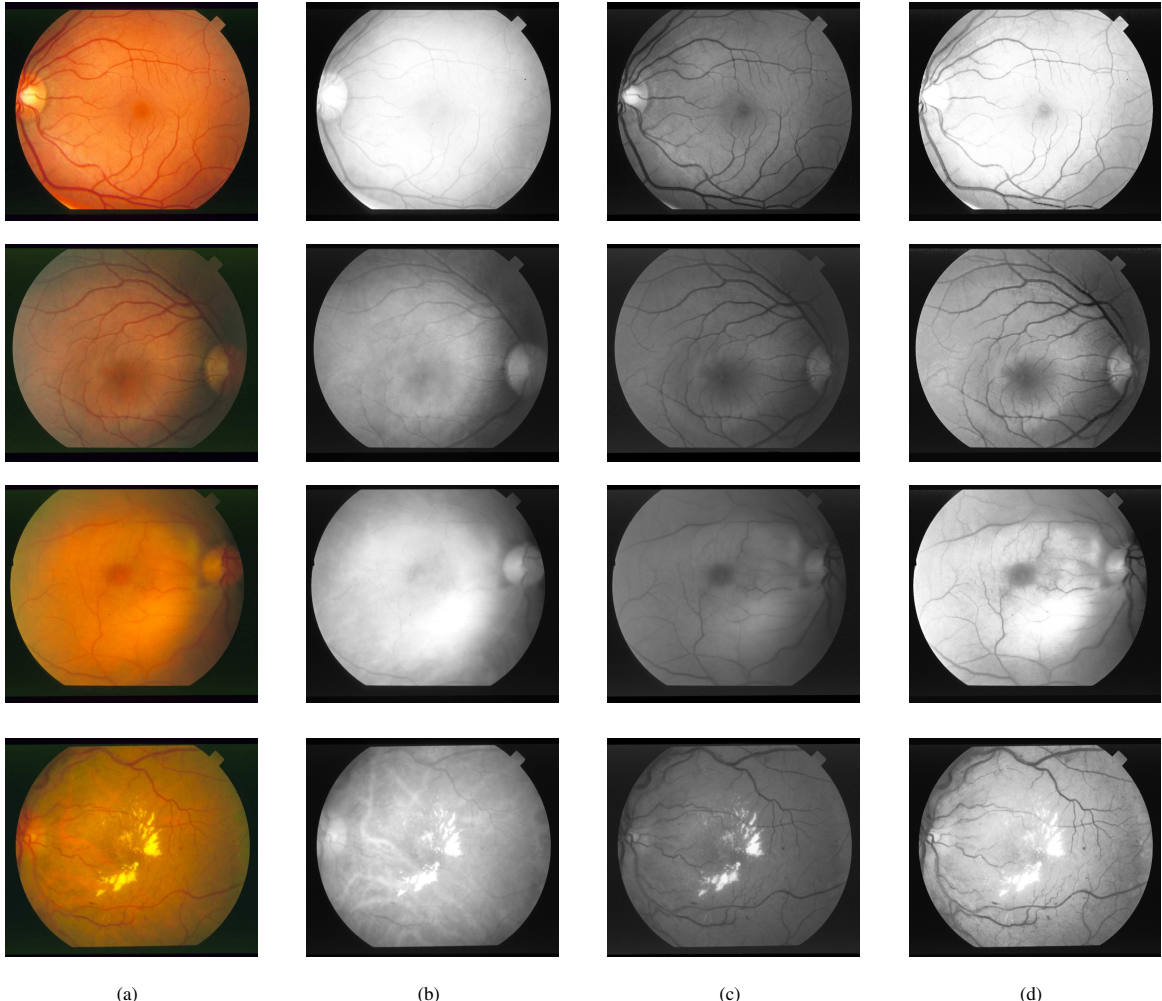


Figure 1. Preprocessing step for normal (top two rows) and abnormal (bottom two rows) images: (a) colour, (b) red channel, (c) green channel, and (d) histogram matched images.

For efficient segmentation of retinal blood vessels, it is desirable to have high contrast between the retinal blood vessels and retinal background whilst there should be low contrast between retinal background and retinal abnormalities. Combining advantages of brightness in red channel and high contrast in green channel results in decreasing the contrast between the abnormalities and the retinal background [26]. This helps to reduce some responses from abnormalities which do not resemble to any blood vessels, that would otherwise decrease the performance of blood vessels segmentation methods.

In our preprocessing step, the histogram matching is used to combine the intensity information from both channels. A histogram matched image is obtained from modifying the histogram of the green channel image using the histogram of the red channel image [26]. Figure 1 shows the effect of this preprocessing step using four images. The first row, where the image is normal and uniformly illuminated, the histogram

matched image still have the information required to segment retinal vessels. While in second and third rows, the vessel in the dark part of the image, on the right side, is now clearly indicated in the histogram matched image than in the green channel image. In the fourth row, the contrast between retinal background and abnormalities is reduced in the histogram matched image than the green channel, these abnormalities gives responses similar to blood vessels when segmenting the retinal vessels.

#### B. Vesselness Measure

Blood vessels can be considered as dark and elongated or line structures - of different diameters and orientations - on a brighter background. Our proposed vesselness measure is based on detecting vessel centerlines and orientation over scales.

In [11], the larger eigenvalue of the Hessian matrix was used as an indicator of the vessel centerline (without using the

absolute value) which is different from the work done in [23], [24], [25]. As vessels are of different diameters, then different scales are used to calculate the eigenvalues and then keeping the maximum response at each image pixel over different scales.

The appropriate local coordinate system in case of line structures is defined by the eigenvectors of the Hessian matrix, matrix of the second order derivatives of the intensity image  $I(x, y)$ . Image derivatives can be taken by convolving the image with derivatives of Gaussian using the Gaussian scale-space techniques [27].

$$L_x = \frac{\partial L(\mathbf{x}, s)}{\partial x} = \frac{1}{2\pi s^2} \int_{\mathbf{x}' \in \mathbb{R}^2} \frac{\partial e^{-\|\mathbf{x}-\mathbf{x}'\|^2/2s^2}}{\partial x} L(\mathbf{x}') d\mathbf{x}' \quad (1)$$

where  $L(\mathbf{x}, s) = I(\mathbf{x}) \otimes G(\mathbf{x}, s)$ ,  $\mathbf{x} = (x, y)'$ ,  $s$  is the scale factor, and  $L_x$  is the image derivative with respect to  $x$ -direction. Mixed and higher order derivatives are computed by taking mixed and higher order derivatives of the Gaussian kernel  $G(\mathbf{x}, s)$ .

Eigenvalues (the larger eigenvalue,  $\lambda_+$ , and the smaller eigenvalue,  $\lambda_-$ , where  $\lambda_+ > \lambda_-$ ) of the Hessian matrix of the intensity image are calculated as [22]:

$$\lambda_+ = \frac{L_{xx} + L_{yy} + \alpha}{2} \quad (2)$$

$$\lambda_- = \frac{L_{xx} + L_{yy} - \alpha}{2} \quad (3)$$

where  $L_{xx}$ ,  $L_{yy}$ , and  $L_{xy}$  are the second derivatives of the intensity image in  $x$ -,  $y$ -, and mixed directions, and  $\alpha = \sqrt{(L_{xx} - L_{yy})^2 + 4L_{xy}^2}$ . Then, the local maximum of the larger eigenvalue  $\lambda_{max}$ , over scales, is calculated as :

$$\lambda_{max} = \max_s [\lambda_+(s)] \quad (4)$$

Figure 2 shows the larger eigenvalue at different scales for a sub-images, as the scale parameter increases, vessels of different diameters can be detected. In this figure, thin vessels (as in bottom of the sub-images) can be detected at small values of  $s$  ( $s = 1$ ), while wider vessels (in the middle) can be detected at bigger values of  $s$  ( $s = 2$  or  $s = 3$ ). Very wide vessels needs larger values for  $s$ .

The orientation in angles,  $\theta$ , are calculated from the eigenvectors of the Hessian matrix as:

$$\hat{e}_+ = \frac{1}{N} \begin{vmatrix} 2L_{xy} \\ L_{yy} - L_{xx} + \alpha \end{vmatrix} \quad (5)$$

$$\hat{e}_- = \frac{1}{N} \begin{vmatrix} L_{yy} - L_{xx} + \alpha \\ -2L_{xy} \end{vmatrix} \quad (6)$$

$$\theta_+ = \tan^{-1} \left[ \frac{L_{yy} - L_{xx} + \alpha}{2L_{xy}} \right] \quad (7)$$

$$\theta_- = \tan^{-1} \left[ \frac{-2L_{xy}}{L_{yy} - L_{xx} + \alpha} \right] \quad (8)$$

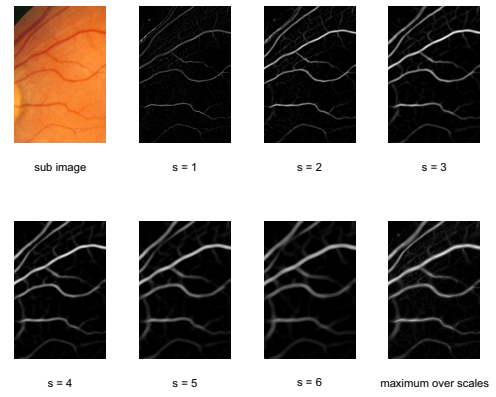


Figure 2. Larger eigenvalue at different scales for a sub-image.

where  $\hat{e}_+$  and  $\hat{e}_-$  are the eigenvectors, and  $\theta_+$  and  $\theta_-$  are the orientations of the corresponding  $\lambda_+$  and  $\lambda_-$ , and  $N = \sqrt{(L_{yy} - L_{xx} + \alpha)^2 + 4L_{xy}^2}$ .

Figure 3 shows eigenvectors corresponding to larger and smaller eigenvalues at different scales. Orientation of the eigenvector that corresponds to the smaller eigenvalue shows the direction of the vessels, while the orientation of the eigenvector that corresponds to the larger eigenvalue shows the direction of the larger changes in the intensity values which represents the perpendicular direction to the vessel.

Directions of eigenvectors corresponding to the smaller eigenvalue at each pixel are depicted in the sub-image for six different scales in Fig. 4. It has also been observed that the variation of the directions of the eigenvectors in a pixel over six different scales is smaller for blood vessel pixels compared with non-blood vessel pixels. Therefore to quantify this variation we use the standard deviation of directions of eigenvectors corresponding to smaller eigenvalues over scales. At vessel centers, the standard deviation of  $\theta_-$ , angle with respect to  $x$ -axis calculated from the eigenvector that corresponds to smaller eigenvalue  $\lambda_-$ , over scales tends towards zero, or a very small value, compared with higher values outside blood vessels. Figure 5 shows a typical and observed probability density function of the standard deviation values of  $\theta_-$  over scales calculated for vessel and non-vessel pixels in a sub-image.

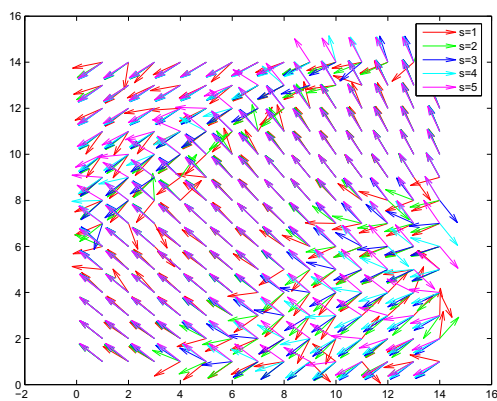
The standard deviation of  $\theta_-$  over scales is calculated as:

$$\sigma_{\theta_-} = std_s [\theta_-(s)] \quad (9)$$

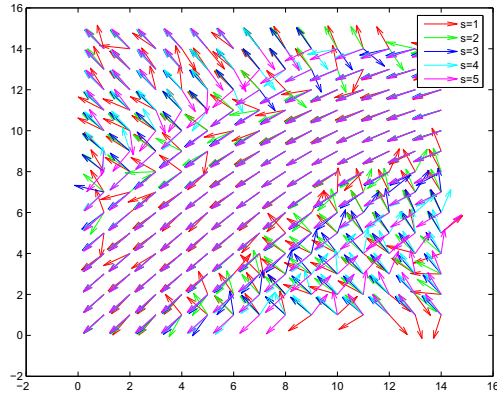
The proposed vesselness measure  $V$  of each pixel is calculated as :

$$V = \frac{\lambda_{max}}{1 + \sigma_{\theta_-}} \quad (10)$$

where  $\lambda_{max}$  is the local maximum of the larger eigenvalue over scales,  $\sigma_{\theta_-}$  is the standard deviation of the  $\theta_-$  over scales. Values of  $\lambda_{max}$  and  $\sigma_{\theta_-}$  have been normalised to be between 0 and 1.



(a)



(b)

Figure 3. Eigenvectors corresponding to (a) larger eigenvalues, and (b) smaller eigenvalues at different scales.

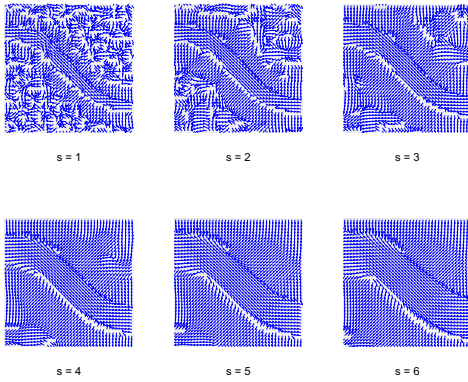


Figure 4. Eigenvectors corresponding to smaller eigenvalues at different scales.

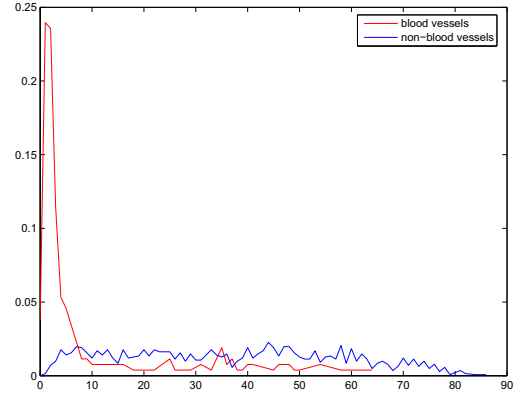


Figure 5. A typical probability density function of the standard deviation values of  $\theta_-$  over scales for vessel and non-vessel pixels.

Equation 10 shows that in our proposed measure we are weighting the information from the vessel centerlines using the orientation of the vessel. In cases where  $\sigma_{\theta_-}$  is a minimum value (equal to 0), then  $V = \lambda_{max}$ . When  $\sigma_{\theta_-}$  has the maximum value (equal to 1) which indicates no blood vessels,  $V = \lambda_{max}/2$ . In this way, we are using information from  $\sigma_{\theta_-}$  to modify the  $\lambda_{max}$  without loosing any information captured by  $\lambda_{max}$ . Typically, the vesselness measure,  $V$ , can be approximated as follows:

$$V = \begin{cases} \lambda_{max}/(1 + \sigma_{\theta_-}), & \text{generally} \\ \lambda_{max}/2, & \text{outside vessels} \\ \lambda_{max}, & \text{within vessels} \end{cases}$$

### III. DATASET

For performance evaluation we use a publicly available dataset [28] consisting of 20 images which are digitized slides captured by a TopCon TRV-50 fundus camera at  $35^\circ$  FOV. Each slide was digitized to produce a  $605 \times 700$  pixels image, standard RGB, 8 bits per colour channel. Every image has been manually segmented by two observers to produce ground truth vessels segmentation. Ten of these images contain pathology and the other ten are normal, giving a good opportunity to test the proposed method in both normal and abnormal retinas. On average, the first observer labelled 32,200 pixels in each image as vessel, while the second observer labelled 46,100 pixels in each image as vessel. Subsequent review indicated that the first person took a more conservative view of the boundaries of vessels and in the identification of small vessels than the second observer [14]. The manual segmentation by the first observer is chosen as the ground truth for vessel segmentation verification in this study.

### IV. EXPERIMENTAL RESULTS

In our experiments, each image is preprocessed using the histogram matching to reduce the contrast between abnormalities and the retinal background as well as to correct the non-uniform illumination in retinal images. Then the

vesselness measure is used for vessel segmentation by finding the local maximum of the larger eigenvalue and the standard deviation of vessel orientations over scales, as in Eq. 10. In our experiments, we calculate maximum over scales up to scale 4 (which was chosen after some exploratory experiments).

The performance is measured with receiver operating characteristic (ROC) curves [29], [30]. An ROC curve plots the false positive rates against the true positive rates, and these rates are defined in the same way as in [14]. The true (false) positive is any pixel which was hand-labelled as a vessel (not vessel), whose intensity is above a given threshold. The true (false) positive rate is established by dividing the number of true (false) positives by the total number of pixels hand-labelled as vessels (not vessels).

From the ROC curves we use the TPR at certain FPR values to compare between our algorithm and other methods in the literature. Also the AUROC (area under the ROC curve) is used as a single measure for performance. The larger is the area under the ROC curve, the better is the performance of the algorithm.

Figure 6 shows two images with their results using the piecewise threshold probing method [14] and the vesselness measure, ROC curves also plotted for these two methods in Fig. 7. For the normal image, the improvement is from FPR >0.05, while for the abnormal image, improvement starts at very low values of FPR. This can be explained as a result of the preprocessing step, where the responses corresponding to abnormalities around the fovea are having lower contrast in the histogram matched image as demonstrated earlier in Fig. 1(d).

On average, when using 20 images, at FPR of 5%, a TPR of 87.43% and 77.31% are achieved for normal and abnormal images respectively. These TPR values increased to 92.69% and 85.90% respectively at FPR of 10%. Table I summarise results obtained when using the vesselness measure.

Table I  
RESULTS FOR VESSELNESS MEASURE (AVERAGED OVER 20 IMAGES)

Image	Specificity	Sensitivity
Normal		87.43%
Abnormal	95%	77.31%
All images		82.37%
Normal		92.69%
Abnormal	90%	85.90%
All images		89.29%
Normal		94.89%
Abnormal	85%	90.11%
All images		92.50%
Normal		96.18%
Abnormal	80%	92.88%
All images		94.53%

For purposes of comparison, the TPR are calculated at FPR of 4.4% for all images, to compare with [13], [14], [16]. We have implemented the algorithm in [13] and used images of the Hoover *et al.* method [14] to find these TPR. Results for Jiang *et al.* were reported in [16]. In addition to the TPR we use the AUROC to compare between our method and results reported by [13], [14], [15], [16], [9], [12]. These results were summarised in Tables II and III.

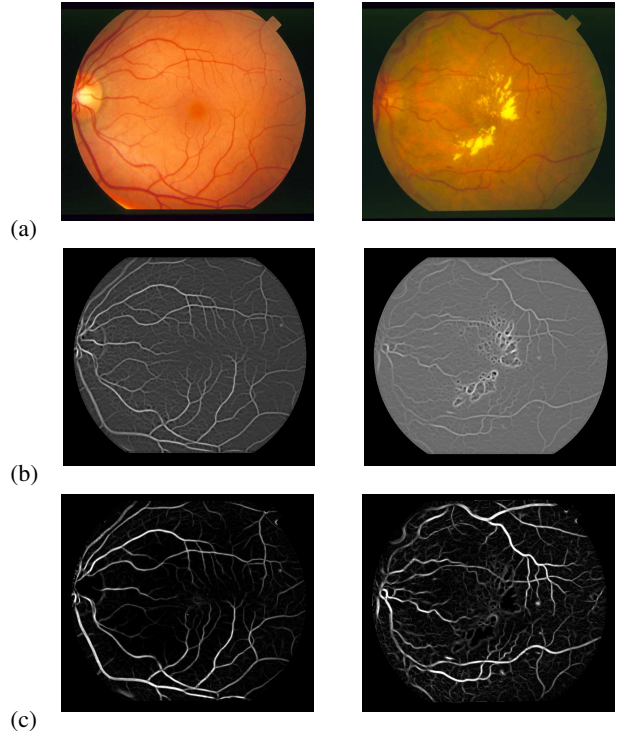


Figure 6. (a) Colour images, (b) Hoover method, and (c) vesselness measure for normal (left) and abnormal (right) images.

Table II  
TPR AT 4.4% FPR (AVERAGED OVER 20 IMAGES)

Method	TPR
2nd Human observer	89.50%
Chaudhuri [13]	55.01%
Hoover [14]	75.48%
Jiang [16]	83.50%
Vesselness measure	80.93%

## V. DISCUSSIONS

It is important to note that in [14], [16], there are five parameters required for these two algorithms, and the reported results are for processing all the 20 image using *ten* and *eight* sets of values for these parameters respectively. While in [15], it depends on an optimisation procedure to select the optimum value for the filter parameters. Significantly, for our proposed algorithm, we need to set only *one* parameter; the scale  $s$ .

The value of the scale  $s$  can be chosen when considering the diameter of blood vessels within a sub-image. It is clear from Fig. 2 that the values  $s = 3$  or  $4$  gives more realistic vessels than the blurred ones at  $s = 5$  or  $6$ . Results using different values of  $s$  are summarised in Table IV.

Results from [9], [12] are better than our results as these are supervised methods which has some advantages over the unsupervised ones, as higher performance. On the other hand, it presents some drawbacks as the need of manually segmented images (ground truth) in order to extract training set and the necessity of a good feature vector in order to classify image pixels to their corresponding classes. There is no doubt that

Table IV  
SENSITIVITY AT 95% SPECIFICITY AND THE AUROC USING DIFFERENT SCALE VALUE (AVERAGED FROM 20 IMAGES)

scale	sensitivity	AUROC
3	81.76%	0.9395
4	82.37%	0.9450
5	81.32%	0.9439
6	79.62%	0.9407

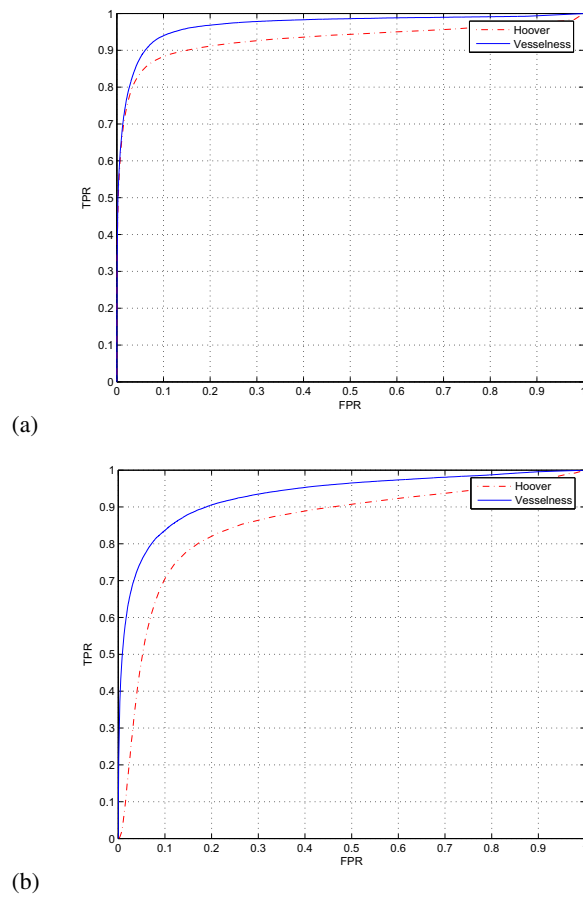


Figure 7. ROC curves for (a) normal, and (b) abnormal images in Fig. 6.

Table III  
AUROC (AVERAGED OVER 20 IMAGES)

Method	AUROC
Chaudhuri [13]	0.8987
Hoover [14]	0.9112
Jiang [16]	0.9298
Al-Rawi[15]	0.9090
Vesselness measure	0.9450
Staal [9]	0.9671
Soares [12]	0.9614

the performance of the classifier is affected by the choice of the feature vector and the training set. Moreover, in our application, where retinal blood vessels segmentation is our main task, generating a training set is not an easy job to do. First, there are 423,500 pixels/image with more than 25% dark background pixels and the dataset consists of 20 images some of them of bad quality (very bright or saturated images). Second, the property of multiple object classes of varying colour/reflectance [16] and sometimes there is a similarity between feature vectors for vessel and non-vessel pixels from different images.

One of the main advantages of our proposed method, it is completely unsupervised, so there is no need for manually

labelled images - segmented by a human observer - which is time consuming to obtain and results depend on to the observer. Another major advantage is that we use a minimum number of parameters, as we need only one parameter in our method in addition to its simplicity and easy implementation.

Our ongoing work is to use results from the vesselness measure in conjunction with classifiers or semi-supervised clustering algorithms. This is achieved by generating a binary image to be used instead of the manually segmented images to train a classifier or as labelled samples for a semi-supervised clustering.

## VI. CONCLUSIONS

A novel unsupervised method for retinal blood vessels segmentation is proposed. This method is based on a proposed vesselness measure, which depends on vessel centerlines and orientations; it requires setting the value of a single parameter. At 5% FPR, retinal blood vessels have been segmented using the proposed unsupervised method with average TPR of 82.4%, our results can be improved by introducing a post processing step to reduce the false positive rates.

## VII. ACKNOWLEDGMENT

The authors would like to thank A. Hoover for making the retinal images publicly available. N. M. Salem would like to acknowledge the financial support of the Ministry of Higher Education, Egypt, for this research.

## REFERENCES

- [1] C. Sinthanayothin, J. F. Boyee, T. H. Williamson, H. L. Cook, E. Mensah, S. Lal, and D. Usher, "Automated detection of diabetic retinopathy on digital fundus images," *Diabetic Medicine*, vol. 19, pp. 105–112, Feb. 2002.
- [2] C. Heneghan, J. Flynn, M. O'Keefe, and M. Cahill, "Characterization of changes in blood vessel width and tortuosity in retinopathy of prematurity using image analysis," *Medical Image Analysis*, vol. 6, pp. 407–429, Dec. 2002.
- [3] F. Zana and J. Klein, "A multimodal registration algorithm of eye fundus images using vessel detection and Hough transform," *IEEE Transactions on Medical Imaging*, vol. 18, pp. 419–428, May 1999.
- [4] A. Can, C. V. Stewart, B. Roysam, and H. L. Tanenbaum, "A feature-based, robust, hierarchical algorithm for registering pairs of images of the curved human retina," *IEEE Transactions on Pattern Analysis and Machine Intelligent*, vol. 24, pp. 347–364, Mar. 2002.
- [5] A. Pinz, S. Bernögger, P. Daltinger, and A. Kruger, "Mapping the human retina," *IEEE Transactions on Medical Imaging*, vol. 17, pp. 606–619, Aug. 1998.
- [6] A. Hoover and M. Goldbaum, "Locating the optic nerve in a retinal image using fuzzy convergence of the blood vessels," *IEEE Transactions on Medical Imaging*, vol. 22, pp. 951–958, Aug. 2003.
- [7] M. Foracchia, E. Grisan, and A. Ruggeri, "Detection of optic disc in retinal images by means of a geometrical model of vessel structure," *IEEE Transactions on Medical Imaging*, vol. 23, pp. 1189–1195, Oct. 2004.

- [8] H. Li and O. Chutatape, "Automated feature extraction in color retinal images by model based approach," *IEEE Transactions on Biomedical Engineering*, vol. 51, pp. 246–254, Feb. 2004.
- [9] J. Staal, M. D. Abràmoff, M. Niemeijer, M. A. Viergever, and B. van Ginneken, "Ridge-based vessel segmentation in color images of the retina," *IEEE Transactions on Medical Imaging*, vol. 23, pp. 501–509, April 2004.
- [10] M. Niemeijer, J. Staal, B. van Ginneken, M. Long, and M. D. Abràmoff, "Comparative study of retinal vessel segmentation methods on a new publicly available database," in *SPIE Medical Imaging*, vol. 5370, pp. 648–656, 2004.
- [11] N. M. Salem and A. K. Nandi, "Segmentation of retinal blood vessels using scale-space features and K-nearest neighbour classifier," in *the 31st International Conference on Acoustics, Speech, and Signal processing - ICASSP '06*, (Toulouse, France), 14–16 May 2006.
- [12] J. V. B. Soares, J. J. G. Leandro, R. M. Cesar-Jr., H. F. Jelinek, and M. J. Cree, "Retinal vessel segmentation using the 2-D Gabor wavelet and supervised classification," *IEEE Transactions on Medical Imaging*, vol. 25, pp. 1214–1222, Sept. 2006.
- [13] S. Chaudhuri, S. Chatterjee, N. Katz, and M. Goldbaum, "Detection of blood vessels in retinal images using two-dimensional matched filters," *IEEE Transactions on Medical Imaging*, vol. 8, pp. 263–269, Sept. 1989.
- [14] A. Hoover, V. Kouznetsova, and M. Goldbaum, "Locating blood vessels in retinal images by piece-wise threshold probing of a matched filter response," *IEEE Transactions on Medical Imaging*, vol. 19, pp. 203–210, Mar. 2000.
- [15] M. Al-Rawi, M. Qutaishat, and M. Arrar, "An improved matched filter for blood vessel detection of digital retinal images," *Computers in Biology and Medicine*, vol. 37, pp. 262–267, Feb. 2007.
- [16] X. Jiang and D. Mojon, "Adaptive local thresholding by verification-based multithreshold probing with application to vessel detection in retinal images," *IEEE Transactions on Pattern Analysis and Machine Intelligent*, vol. 25, pp. 131–137, Jan. 2003.
- [17] D. Wu, M. Zhang, J. Liu, and W. Bauman, "On the adaptive detection of blood vessels in retinal images," *IEEE Transactions on Biomedical Engineering*, vol. 53, pp. 341–343, Feb. 2006.
- [18] Y. A. Tolias and S. M. Panas, "A fuzzy vessel tracking algorithm for retinal images based on fuzzy clustering," *IEEE Transactions on Medical Imaging*, vol. 17, pp. 263–273, April 1998.
- [19] T. McInerney and D. Terzopoulos, "T-snakes: topology adaptive snakes," *Medical Image Analysis*, vol. 4, pp. 73–91, June 2000.
- [20] F. Zana and J. C. Klein, "Segmentation of vessel-like patterns using mathematical morphology and curvature evaluation," *IEEE Transactions on Image Processing*, vol. 10, pp. 1010–1019, July 2001.
- [21] A. M. Mendonça and A. Campilho, "Segmentation of retinal blood vessels by combining the detection of centerlines and morphological reconstruction," *IEEE Transactions on Medical Imaging*, vol. 25, pp. 1200–1213, Sept. 2006.
- [22] M. E. Martínez-Pérez, A. Hughes, A. Stanton, S. Thom, A. Bharath, and K. Parker, "Scale-space analysis for the characterisation of retinal blood vessels," in *Medical Image Computing and Computer-Assisted Intervention - MICCAI '99* (C. Taylor and A. Colchester, eds.), pp. 90–97, 1999.
- [23] A. F. Frangi, W. J. Niessen, K. L. Vincken, and M. A. Viergever, "Multiscale vessel enhancement filtering," in *Medical Image Computing and Computer-Assisted Intervention - MICCAI '98* (W. M. Wells, A. Colchester, and S. L. Delp, eds.), pp. 130–137, 1998.
- [24] Y. Sato, S. Nakajima, N. Shiraga, H. Atsumi, S. Yoshida, T. Koller, G. Gerig, and R. Kikinis, "3D multi-scale line filter for segmentation and visualization of curvilinear structures in medical images," in *CVRMed-MRCAS '97, Lecture Notes in Computer Science* (J. Troccaz, E. Grimson, and R. Mösges, eds.), vol. 1205, pp. 213–222, Springer-Verlag, Berlin Heidelberg, 1997.
- [25] C. Lorenz, I.-C. Carlsen, T. M. Buzug, C. Fassnacht, and J. Weese, "Multi-scale line segmentation with automatic estimation of width, contrast and tangential direction in 2D and 3D medical images," in *CVRMed-MRCAS '97, Lecture Notes in Computer Science* (J. Troccaz, E. Grimson, and R. Mösges, eds.), vol. 1205, pp. 233–242, Springer-Verlag, Berlin Heidelberg, 1997.
- [26] N. M. Salem and A. K. Nandi, "Novel and adaptive contribution of the red channel in pre-processing of colour fundus images," *Journal of the Franklin Institute, Special Issue: Medical Applications of Signal Processing, Part I*, vol. 344, pp. 243–256, 2007.
- [27] T. Lindeberg, *Scale-space Theory in Computer Vision*. Netherlands: Kluwer Academic publisher, 1994.
- [28] "The STARE project." <http://www.ces.clemson.edu/~ahoover/stare>.
- [29] C. E. Metz, "Basic principles of ROC analysis," *Seminars Nucl. Med.*, vol. 8, no. 4, pp. 283–298, 1978.
- [30] T. Fawcett, "ROC graphs: notes and practical considerations for researchers," Tech. Rep. HPL-2003-4, HP Laboratories, 2004.